Check for updates

Advanced hybrid silica nanoparticles with pH-responsive diblock copolymer brushes: optimized design for controlled doxorubicin loading and release in cancer therapy

Shatha Lahmadi,†[a] Salman Alamery,†[b] Abeer Beagan,[a] Khalid Alotaibi[a] and Abdullah Alswieleh (ID) *[a]

This study delves into the development, characterization, and application of modified mesoporous silica nanoparticles (MSNs) for targeted drug delivery in cancer therapy. MSNs were functionalized with poly(2-(diisopropylamino)ethyl methacrylate) (PDPA) and poly(glycidyl methacrylate) (PGMA), and further modified with cross-linkers DAE and Ornithine. Characterization using FT-IR, SEM, TEM, DLS, and XPS confirmed the successful surface modifications, revealing particle sizes primarily within the 63–94 nm range. The MSNs demonstrated a pH-responsive behavior, crucial for smart drug delivery. Loading and release studies using Doxorubicin (DOX) showed a controlled release, with an 8 µg mg^{-1} loading capacity. Cytotoxicity assays on Caco2 colon cancer cells revealed that unloaded nano-systems, at concentrations above 45 µM, resulted in approximately 60% cell death, indicating inherent anti-cancer properties. However, variations in cytotoxic effects were observed in drug-loaded MSNs, with some modifications showing reduced anti-cancer activity. These findings highlight the potential of MSNs in drug delivery and cancer treatment, emphasizing the importance of nanoparticle design in therapeutic efficacy.

1 Introduction

In recent times, there has been significant progress in the development of nanomaterials within the field of nanomedicine.[1,2] Researchers aim to overcome the limited effectiveness and adverse side effects associated with direct administration of anticancer agents in cancer treatment.[3,4] To address these challenges, a diverse range of nanoparticles with a radius smaller than 100 nm have been engineered as drug carriers, offering potential solutions to enhance therapeutic outcomes and minimize complications.[5,6] Notably, nanoparticles, such as gold,[7] carbon,[8] polymeric[9] and mesoporous silica nanoparticles (MSNs)[10] have emerged as promising delivery systems. MSNs, in particular, have garnered significant attention due to their capacity to efficiently encapsulate therapeutic drugs or imaging agents for cancer treatment and diagnostic imaging purposes.[10,11] Moreover, MSNs possess favorable characteristics that position them as highly viable candidates for drug delivery applications, including their large surface area, robustness against thermal and mechanical conditions, and biocompatibility.[12,13]

The surface chemistry of MSNs can be precisely engineered, offering a crucial factor for achieving accurate administration of the Doxorubicin drug. To enhance drug delivery systems, the combination of MSNs with a polymeric shell has been developed, particularly through the incorporation of stimuli-responsive polymer brushes.[14,15] These polymer chains, arranged in a brush-like conformation, are tethered to the surface of MSNs, playing a vital role in either safeguarding or facilitating the controlled release of cargo based on internal or external environmental stimuli, such as changes in pH,[16] redox reactions,[17] exposure to light,[18] or ultrasound.[19] When these stimuli is applied, the polymer brushes can effectively modulate the diffusion of drugs through the nanopores and polymer chains, thereby improving the precision and efficiency of drug delivery.

pH-Responsive polymers possess the unique ability to undergo conformational changes or alterations in hydrophilicity in response to local pH conditions.[20,21] This characteristic is harnessed to prevent premature drug release, taking advantage of the pH disparity between healthy and cancerous tissues.[22,23] In our previous investigations, we successfully synthesized MSNs coated with poly(2-(diethylamino)ethyl methacrylate) as pore caps, enabling the loading of DOX.[24,25]

[a]Department of Chemistry, College of Science, King Saud University, Riyadh, Kingdom of Saudi Arabia. E-mail: aswieleh@ksu.edu.sa

[b]Department of Biochemistry, College of Science, King Saud University, Riyadh, Kingdom of Saudi Arabia

† These authors contributed equally to this work and share first authorship.

To specifically target breast cancer cells, folic acid molecules were conjugated to the nanosystem. Interestingly, our findings revealed that under acidic conditions, the system exhibited controlled release of DOX, while exhibiting minimal release at physiological pH. This selectivity was attributed to the overexpression of folate receptors on breast cancer cells, making our folic acid conjugate system highly effective in their targeted elimination.[24] In order to overcome the challenge of nonspecific and uncontrolled delivery of arsenic trioxide and paclitaxel, researchers have developed a novel approach by modifying mesoporous silica nanoparticles (MSNs) with pH-sensitive lipids and polyacrylic acid.[26] This innovative nanosystem design effectively mitigated undesired drug release and demonstrated remarkable efficacy in targeting MCF-7 cancer cells. A multi-functionalized mesoporous silica KIT-6-based nanocarrier, incorporating guanidinium ionic liquid (GuIL) in inner surface, and PEGylated folic acid (PEG-FA) and polyethylene imine (PEI) on the outer surface, was designed for efficient delivery of anti-EGFR1 siRNAs to MD-MBA-231 cell line.[27] The nanocarrier enhanced the cytotoxic effect, highlighting the potential of this nanocarrier for targeted therapy in triple-negative breast cancer.

To improve the efficiency of the drug release, cross-linked polymer chains could improve the release of target molecules by forming physical or chemical interactions.[28,29] Inspired by these designs, we prepared MSNs modified with pH-responsive diblock copolymer of poly(2-(diisopropylamine) ethyl methacrylate) and poly(glycidyl methacrylate) as DOX nanocarriers. The presence of the amino and epoxy groups on the side chain of the diblock copolymer would confer the pH-responsive character and provide the ability to cross-link the polymer chains using ethylenediamine and ornithin molecules, acting as gatekeepers to protect/promote the loading and release of DOX (Scheme 1). The effect of cross-linking degree on DOX loading/release and cytotoxicity are also reported.

2 Materials and methods

2.1. Material

3-Aminopropyl triethoxysilane (APTES, 99%), 2,2′-bipyridyl (bipy, ≥99%), 2-bromo-2-methylpropionyl bromide (BIBB, 98%), dichloromethane (DCM, HPLC grade), ethanol (EtOH, ≥99.8%), ethylenediamine (1,2-diaminoethane, DAE, ≥99%), methanol (MeOH, ≥99.8%), hexadecyltrimethylammonium bromide (CTAB, ≥98%), glycidyl methacrylate (GMA, 97%), 2-(diisopropylamino)ethyl methacrylate) (DPA, 97%), and tetraethoxysilane (TEOS, 98%) were purchased from Sigma-Aldrich. Cupric bromide ($CuBr_2$, 98%), cuprous chloride (CuCl, 96%), and potassium dihydrogen orthophosphate (KH_2PO_4, 99%) were provided by BDH chemicals. Ascorbic acid (98%), and L(+)-ornithine monohydrochloride (Orn, 99%) were obtained from Riedel-de Haën. Ammonium chloride (NH_4Cl) was supplied by Avonchem Ltd. Triethylamine (TEA, 99%) was purchased from Loba Chemie. Doxorubicin hydrochloride (DOX) was provided by Tokyo Chemical Industry (TCI). Sodium hydroxide (NaOH) was obtained from Central Drug House (CDH). In all experiments, distilled water was used from Gesellschaft für Labortechnik mbH, Model 2002 – single distillation water stills.

2.2. Characterization

Several techniques were employed to confirm the successful formation of the nanosystem. Fourier Transform Infrared (FTIR) spectra were recorded using a PerkinElmer Spectrum BX instrument, covering the range of 400–4400 cm^{-1}. Thermogravimetric Analysis (TGA) curves were obtained at a heating rate of 20 °C min^{-1}, within a temperature range of 25–600 °C, using a PerkinElmer Pyris 1 TGA instrument. X-ray Photoelectron Spectroscopy (XPS) analyses were conducted on a JEOL JPS-9030 photoelectron spectrometer. The morphology and particle size were examined by Scanning Electron Microscopy (SEM) using a JEOL JSM-7610F instrument at 15 kV, and by Transmission Electron Microscopy (TEM) on a JEOL JEM-1400. The hydrodynamic size and zeta potential of the samples were measured at various pH levels using Dynamic Light Scattering (DLS) on
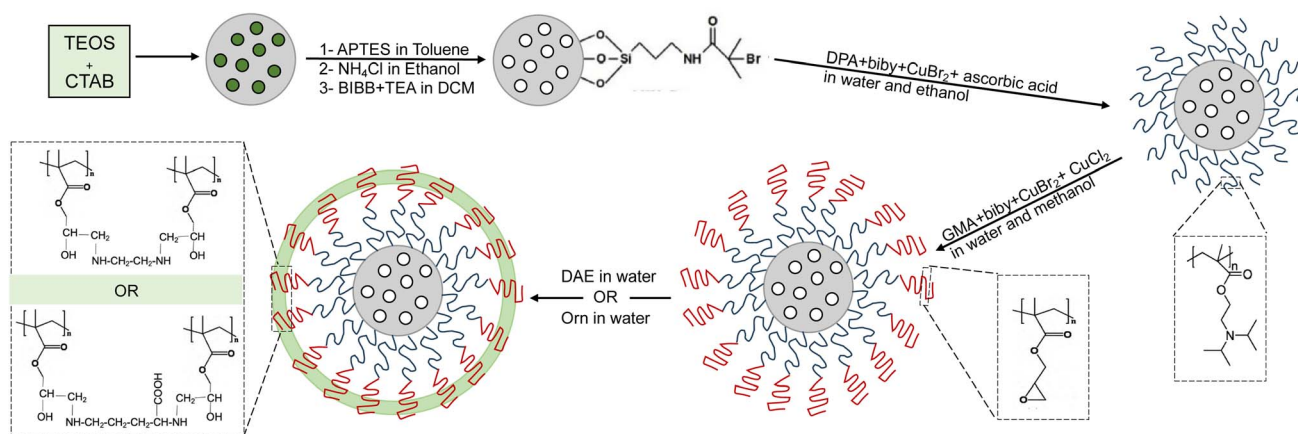
Scheme 1 Schematic presentation of the synthesis route of the multifunctional hybrid silica nanoparticles grafted with pH-responsive diblock copolymer brushes.

a Malvern Instruments Zetasizer Nano ZS at 25 °C. Drug loading capacity and release profiles were quantified using a UV-vis spectrophotometer.

2.3. Methods

2.3.1. Preparation of MSNs with a diameter of 50–80 nm.
CTAB (1.1 g) was dissolved in 326 mL of buffer solution (pH 7, composed of 6.8 g KH_2PO_4 and 0.89 g NaOH) and sonicated for 15 min. Subsequently, 5.3 mL of TEOS was added dropwise, and the mixture was stirred at 40 °C for 8 h. The resulting white solid nanoparticles were collected by centrifugation at 6000 rpm for 10 min and subsequently washed with water and ethanol.

2.3.2. Modification of MSNs with CTAB with amino groups (MSNs-NH2 with CTAB).
1.5 g of MSNs was suspended in 50 mL of methanol, sonicated for 10 min, followed by the addition of 1.5 mL of APTES. The mixture was then heated to 65 °C and stirred for 24 h. The resultant white solid was washed three times with ethanol.

2.3.3. Extraction of CTAB template from MSNs-NH$_2$ with CTAB.
0.4 g of MSNs-NH$_2$ with CTAB was suspended in 40 mL of a 40 mM ammonium chloride/methanol solution. The mixture was sonicated for 3 h at 70 °C, and the white solid was subsequently washed three times with ethanol.

2.3.4. Surface initiation of MSNs-NH$_2$.
1 g of MSNs-NH$_2$ was dispersed in 25 mL of DCM and sonicated for 10 min. Then, 0.5 mL of TEA and 0.25 mL of BIBB were added, and the mixture was stirred overnight. MSNs-Br was washed five times with DCM and three times with ethanol.

2.3.5. Preparation of copolymer brushes on the surface of MSNs.
Initially, 0.4 g of MSNs-Br was dispersed in an ethanol–water mixture (4 : 1) under a nitrogen atmosphere for 30 min. A mixture containing 0.5 mL of PDPA, 6.7 mg of bipy, 0.9 mg of $CuBr_2$, 8 mL of ethanol, and 2 mL of water was then added and kept under nitrogen for an additional 15 min. Finally, 7.6 mg of ascorbic acid was introduced to initiate polymerization, which proceeded for 3 h at room temperature under a nitrogen atmosphere. MSNs-PDPA was washed with water and ethanol. For the second polymerization step, MSNs-PDPA was re-dispersed in a methanol–water mixture (3 : 1) with 2.5 mL of GMA under nitrogen. After 30 min, 1.92 mg of $CuBr_2$, 70.5 mg of bipy, and 18.2 mg of CuCl were added, and the mixture was polymerized for 2 h at room temperature. Finally, MSNs-PDPA-*co*-PGMA was washed with water and methanol.

2.3.6. Cross-linking of MSNs-PDPA-*co*-PGMA brush copolymer.
Cross-linking was performed using ethylenediamine or L(+)-ornithine. Specifically, 300 mg of MSNs-PDPA-*co*-PGMA was suspended in 20 mL of alkaline solution (pH 9), followed by the gradual addition of 5 mL of a 1 or 3 µM crosslinker solution. The reaction stirred overnight at 90 °C. The X-linked MSNs-PDPA-*co*-PGMA was then washed with water and methanol.

2.4. Drug loading and release

A DOX solution was prepared by dissolving 5 mg of DOX in 10 mL of acidic PBS (pH 3). Then, 1 mL of this solution was added to 1 mg of the sample and shaken for 24 h in dark conditions. The pH of the mixture was altered to alkaline (pH 9) using alkaline PBS. Cumulative release before and after cross-linking at pH values of 6, 6.5, and 7.4 was estimated by suspending 0.25 mg of the sample in 1 mL of the selected medium, followed by incubation in a shaking incubator at 37 °C with a speed of 100 rpm. At specified intervals, the samples were centrifuged, the supernatant was removed for analysis, and replaced with fresh solution.

2.5. Cell cytotoxicity assay

The cytotoxicity of all samples on Caco2 cells was evaluated using an MTT assay. Cancer cells were seeded in a 96-well plate at a density of 3×10^3 cells per well and incubated at 37 °C for 24 h. The growth media was then replaced with various concentrations of the samples (ranging from 733 µM to 3 µM). After 24 h, MTT reagent was added to each well, followed by incubation for 3 h. The resulting MTT-formazan crystals were dissolved in DMSO, and the absorbance was measured at 405 nm using a microplate reader.

3 Results and discussion

3.1. Nanomaterials characterizations

The surface modifications of the mesoporous silica nanoparticles (MSNs) were comprehensively characterized using Fourier Transform Infrared (FTIR) spectroscopy. The FTIR spectra of various MSN formulations, including MSNs with CTAB, MSNs without CTAB, MSNs-Br, MSNs-PDPA, and MSNs-PDPA-*co*-PGMA, were analyzed (Fig. 1). Characteristic peaks around 1080, 800, and 460 cm^{-1} were identified, corresponding to the Si–O bond, indicative of the silica-based structure of the nanoparticles. Additionally, the absorption bands in the 3300–3600 cm^{-1} region and at 950 cm^{-1} were attributed to the hydroxyl O–H stretch, which are typically present on the surface of silica materials. The FTIR spectra also displayed stretching peaks at 2930 cm^{-1} and 2860 cm^{-1}, associated with the CTAB
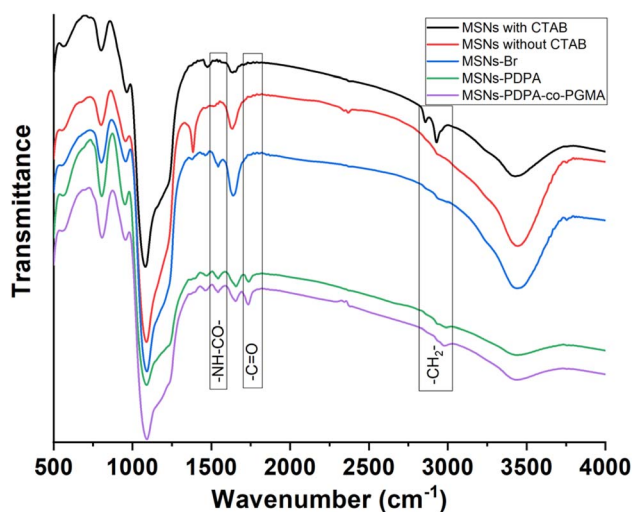

Fig. 1 FT-IR spectra of the fabricated nanoparticles: MSNs with CTAB (black), MSNs without CTAB (red), MSNs-Br (blue), MSNs-PDPA (green) and MSNs-PDPA-*co*-PGMA (purple).

molecule. These peaks' absence in the spectra following CTAB removal confirms the effective elimination of CTAB, validating the removal process. After the initiation step, the appearance of a peak at 1545 cm^{-1} corresponding to the –NH–CO– group suggested the successful introduction of this functional group. This change is critical as it implies successful functionalization, a step essential for the subsequent polymerization processes. Furthermore, in the spectra of MSNs-PDPA, the presence of a carbonyl group peak at 1736 cm^{-1} indicates that PDPA was successfully grafted onto the surface of MSNs-Br. The presence and intensity of this peak are crucial, as they demonstrate the successful attachment of the PDPA onto the MSN surface, a foundational aspect for the development of the final nano-composite. Notably, the intensity of the carbonyl group in the MSNs-PDPA-*co*-PGMA spectra increased following co-polymerization with PGMA. This increase in intensity may be attributed to the added density of carbonyl groups introduced by PGMA, suggesting an effective co-polymerization process.

The efficiency of anti-cancer drug encapsulation in nano-particles is significantly influenced by the size and morphology of the nanoplatforms. In biomedical applications, it's crucial for these nanoplatforms to have a size smaller than 200 nm to ensure optimal cellular uptake and biodistribution.[30] Accordingly, the morphologies and sizes of the fabricated nano-particles were meticulously studied using Transmission Electron Microscopy (TEM) and Scanning Electron Microscopy (SEM), as depicted in Fig. 2.

Observations from TEM and SEM revealed that the MSNs, post-CTAB extraction, formed small-sized grains ranging from 63 to 78 nm, with a pore size of approximately 2.3 nm, and exhibited well-dispersed, regularly spherical shapes (Fig. 2A and B). This size range is particularly favorable for biomedical applications due to enhanced cellular uptake and reduced clearance by the reticuloendothelial system. In MSNs-PDPA samples, as per the SEM images, the average particle size marginally increased to about 85 nm, which could be attributed to the additional layer of PDPA on the MSNs surface. The average dry thickness of the PDPA brushes was estimated to be around 13 nm. Furthermore, Fig. 2D illustrates that the average particle size of MSNs-PDPA-*co*-PGMA was approximately 94 nm, suggesting a slight increase due to the copolymerization with PGMA. These findings highlight the precise control achieved in nanoparticle synthesis, ensuring that the size remains within an optimal range for drug delivery applications. The observed increase in size following each modification step provides insight into the layer-by-layer construction of these complex nanostructures.

Dynamic Light Scattering (DLS) was employed to assess the particle size and surface zeta potential of the synthesized nanoparticles, with the findings depicted in Fig. 3. The DLS data revealed that both the size and surface zeta potential of the particles are influenced by the pH variation of the solution. Notably, for all samples analyzed, the average DLS diameter increased within the pH range of 6.5 to 7.5, aligning with the pK_a value of PDPA. This behavior suggests a dependence of particle size on the chain length and the hydrophobic PDPA to hydrophilic PGMA mass ratio. Post cross-linking with DAE and

Orn, a reduction in the diameters of MSNs-PDPA-*co*-PGMA was observed. In basic media, the sizes of the diblock polymers (including MSNs-PDPA-*co*-PGMA, and those cross-linked with DAE and Orn) ranged from 100 to 140 nm. It's noteworthy that the SEM-measured sizes of these diblock polymer samples were smaller than those obtained by DLS, a discrepancy likely explained by the measurement of hydrodynamic diameter in solution for DLS, as opposed to the dry conditions under which SEM images were captured.

Surface charge, as indicated by zeta potential measurements at different pH levels, varied across the samples (Fig. 3B). For all surfaces, except MSNs-PDPA-*co*-PGMA, an increase in surface zeta potential was noted as the pH decreased from 7.5 to 6.5. This trend is attributed to the protonation of amine groups in PDPA, DAE, and Orn. Interestingly, MSNs-PDPA-*co*-PGMA X-linked with Orn exhibited a negative charge at pH levels above 7.5, likely due to the deprotonation of amine and carboxylic acid groups in Orn. In contrast, the zeta potential of MSNs-PDPA-*co*-PGMA brushes remained relatively stable, at approximately 10 mV, across the studied pH range. This stability may be linked to the presence of hydroxyl groups on the particle surface.

The chemical composition of the coatings was precisely determined using X-ray Photoelectron Spectroscopy (XPS), as illustrated in Fig. 4. The C 1s XPS narrow-scan spectrum of MSNs-PDPA (Fig. 4A) revealed four distinct peaks of carbon atoms: [C–C/C–H] at 284.8 eV, [C–N] at 285.9 eV, [C–O] at 286.6 eV, and [O=C–O] at 289.2 eV. The peak area ratios were observed as 3.5 : 2.7 : 1.2 : 1, respectively, compared to the theoretical peak ratios of 7 : 3 : 1 : 1 for these respective carbon atom environments. In the XPS C 1s narrow scan of MSNs-PDPA-*co*-PGMA (Fig. 4B), four peaks were identified: [C–C/C–H] at 284.8 eV, [C–N] at 285.8 eV, [C–O] at 286.4 eV and [O=C–O] at 289.1 eV, with a ratio of 2.9 : 3.8 : 2.4 : 1.0. These findings shows that there was an increase in peak area of [C–O], indicating a successful copolymerization. The fitted ratio in the XPS C 1s narrow scan of MSNs-PDPA-*co*-PGMA X-linked with DAE (Fig. 4C) showed peaks at [C–C/C–H] 284.8 eV, [C–N] 285.9 eV, [C–O] 286.6 eV, and [O=C–O] 288.9 eV, with respective peak ratios of 3.7 : 3.8 : 2.7 : 1.0. The noticeable increase in the [C–N] peak at 285.9 eV can be attributed to the successful reaction between DAE molecules and PGMA segments. Similar observations were noted in MSNs-PDPA-*co*-PGMA X-linked with Orn, with peaks at [C–C/H] 285.0 eV, [C–N] 285.9 eV, [C–O] 286.6 eV, and [O=C–O] 288.9 eV, suggesting a successful cross-linking process. Fig. 4E shows the XPS N 1 s spectra of the MSNs-PDPA, MSNs-PDPA-*co*-PGMA, MSNs-PDPA-*co*-PGMA cross-linked with DAE, and MSNs-PDPA-*co*-PGMA cross-linked with Orn. In the N 1s spectrum, a single peak is observed at 401.2 eV, corresponding to the [C–N] species present in the PDPA and PDPA-*co*-PGMA layers. After the reaction with DAE and Orn, the XPS spectrum exhibits notable changes. Two peaks are observed with binding energies at 399 eV and 401.4 eV, which are associated with the [–NH] and [C–N] species, respectively. These changes indicate the successful incorporation of DAE and Orn, resulting in the formation of additional nitrogen-containing functional groups in the nanoparticles.
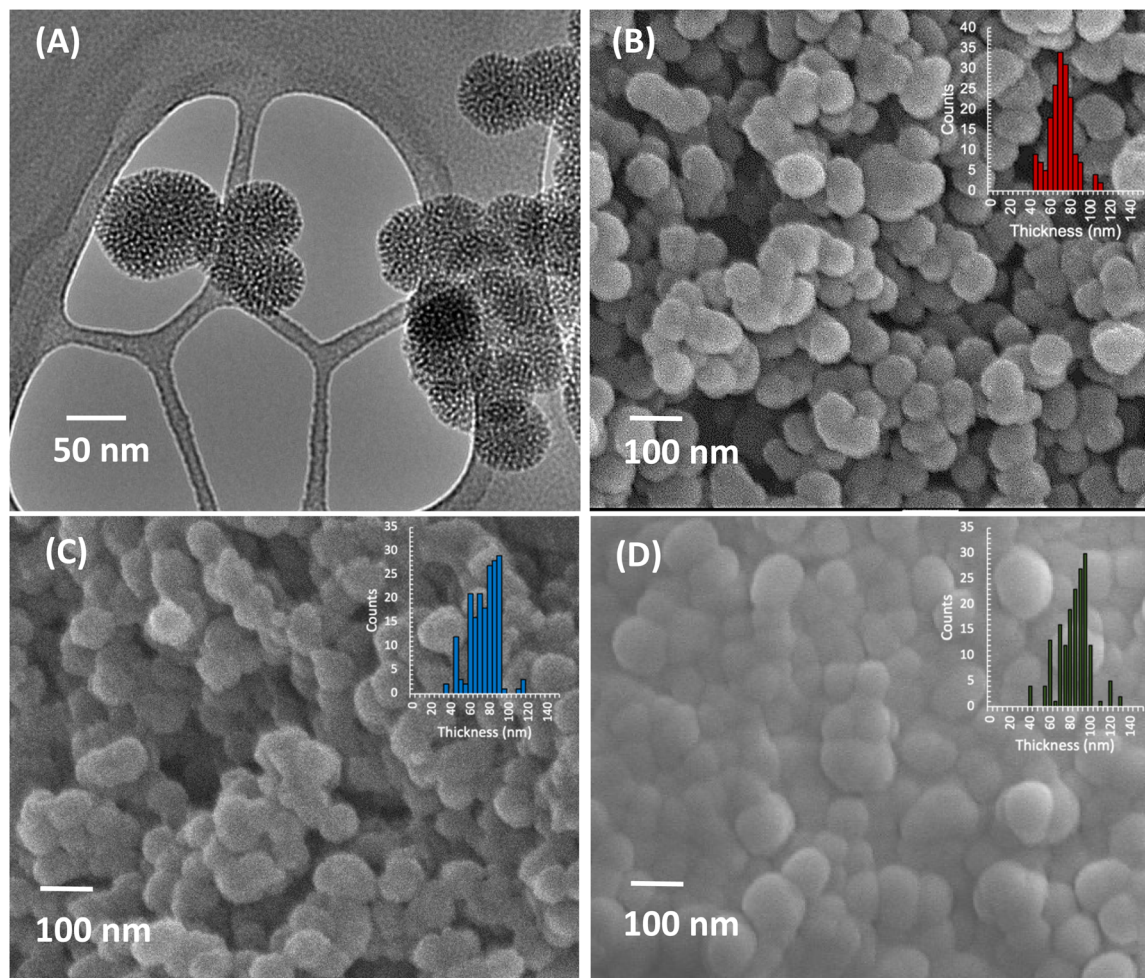
Fig. 2 (A) TEM image of MSNs after CTAB extraction, (B) SEM image of MSNs after CTAB extraction, (C) SEM image of MSNs–PDPA and (D) SEM image of MSNs–PDPA-*co*-PGMA.

3.2. Drug loading and release

The study next explored the pH-dependent gatekeeper behavior of the grafted diblock polymers on the MSNs surface, controlled by the PDPA brushes. It is hypothesized that in acidic environments, the PDPA brushes become positively charged and hydrophilic, leading to the opening of the MSNs pores. Conversely, in basic solutions, these brushes become neutralized and hydrophobic, resulting in pore closure. Additionally,
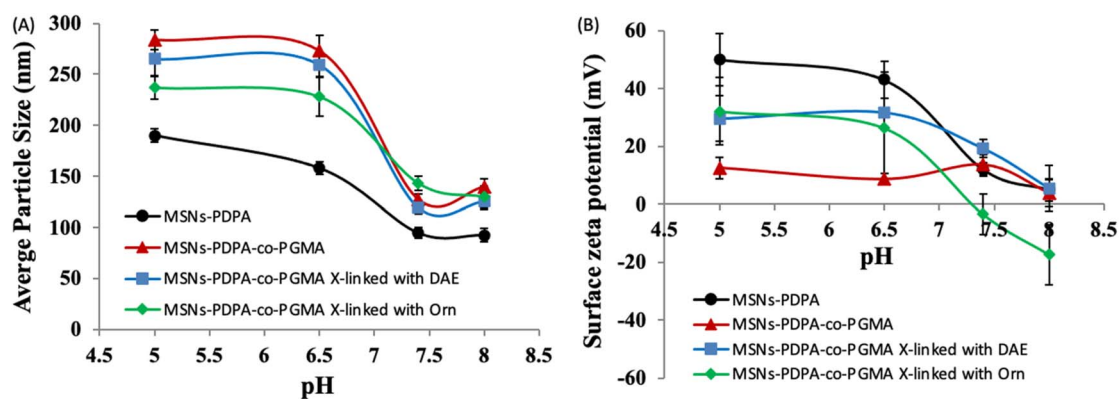

Fig. 3 The changes in particle size (A) and zeta potential (B) of the fabricated nanoparticles (MSNs–PDPA, MSNs–PDPA-*co*-PGMA, MSNs–PDPA-*co*-PGMA X-linked with DAE and MSNs–PDPA-*co*-PGMA X-linked with Orn) at different pH of the solutions.
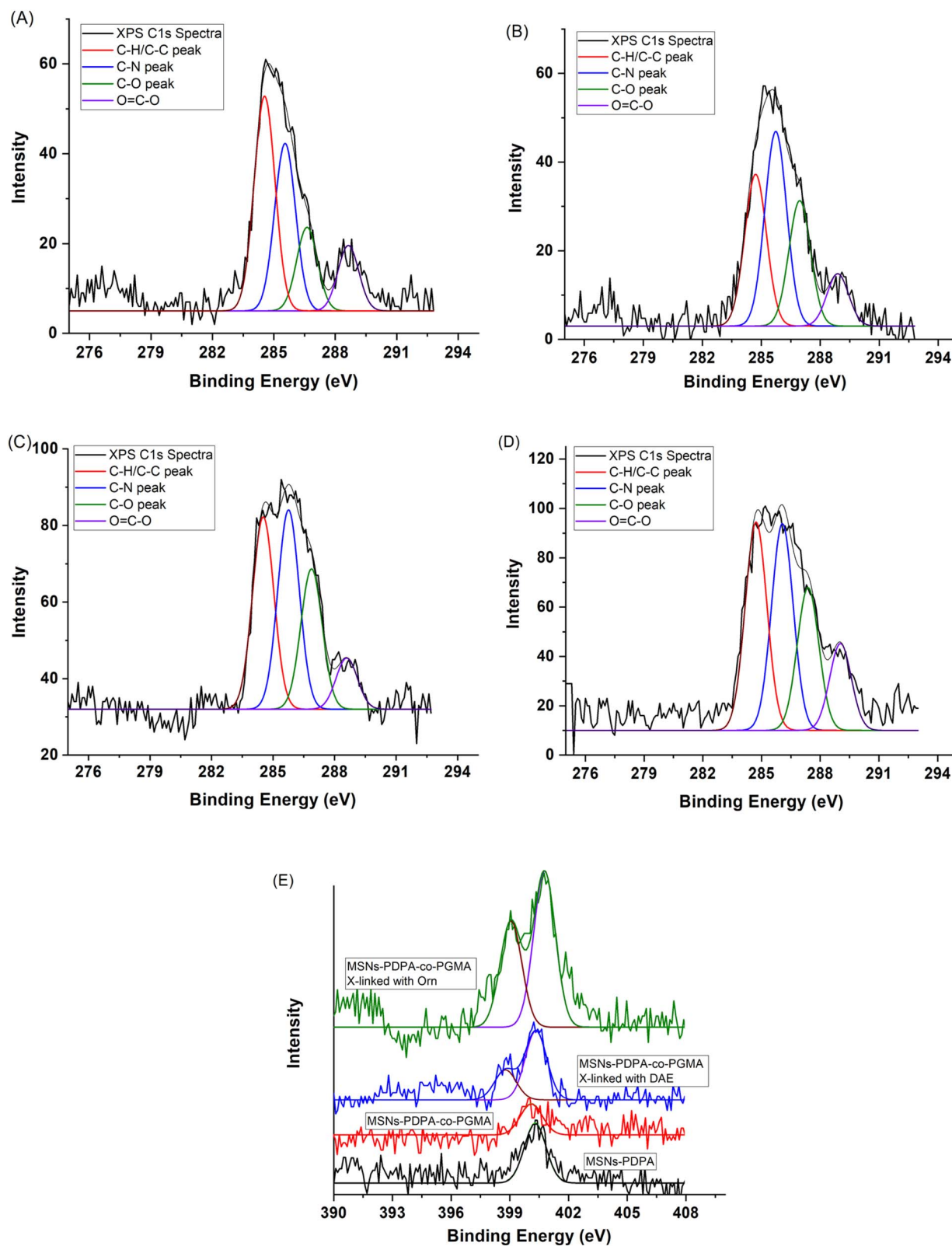
Fig. 4   X-ray photoelectron spectroscopy (XPS) C 1s spectra of: (A) MSNs-PDPA; (B) MSNs-PDPA-*co*-PGMA; (C) MSNs-PDPA-*co*-PGMA X-linked with DAE and (D) MSNs-PDPA-*co*-PGMA X-linked with Orn. (E) XPS N 1s spectra of all fabricated samples.

the amine groups in the cross-linkers (DAE and Orn) are expected to become protonated and positively charged in acidic media.

The controlled drug release behavior of the MSNs-PDPA-*co*-PGMA, and its derivatives cross-linked with DAE and Orn, was investigated using DOX as a model cancer drug. Initially, DOX was loaded into the samples at pH 3, after which the loaded nanoparticles were isolated and washed with alkaline PBS buffer (pH 9) to close the pores. The loading capacity was determined to be approximately 8 μg mg^{-1} for each nanoparticle type. The subsequent release of DOX from these samples was studied at varying pH levels. Generally, an increased rate of DOX release was observed with the decrease in buffer pH (pH 7.4, 6.5, and 6.0), as shown in Fig. 5.

Surprisingly, no significant difference in DOX release from MSNs-PDPA-*co*-PGMA was observed across the different pH levels. In contrast, MSNs-PDPA-*co*-PGMA cross-linked with DAE and Orn exhibited the highest cumulative drug release at pH 6 and the lowest at pH 7.4. This variation in drug release can be attributed to the protonation of amino groups within both polymer segments and the DOX molecule itself. Notably, the drug release from MSNs-PDPA-*co*-PGMA cross-linked with Orn was slower in acidic conditions, potentially due to the charge interactions between DOX and the carboxylic groups in Orn.

3.3. Cell cytotoxicity assay

The cytotoxicity effects of various nano-systems were evaluated using the Caco2 colon cancer cell line, treated with different concentrations of both loaded and unloaded formulations: MSNs-PDPA-*co*-PGMA, MSNs-PDPA-*co*-PGMA X-linked with DAE, and MSNs-PDPA-*co*-PGMA X-linked with Orn. Free DOX served as a positive control. As depicted in Fig. 6, free DOX demonstrated the anticipated cytotoxic effect, significantly reducing cell viability. Interestingly, the unloaded nano-systems, including all three MSN variants, exhibited cytotoxic effects, leading to approximately 60% cell death at concentrations above 45 μM. This suggests that the nano-systems themselves, without drug loading, possess inherent anti-cancer properties. Conversely, the loaded MSNs-PDPA-*co*-PGMA showed reduced cytotoxicity compared to its unloaded counterpart, indicating that the presence of DOX within the nano-systems might alter their interaction with cancer cells. A notable observation was that the loaded MSNs-PDPA-*co*-PGMA X-linked with DAE and Orn demonstrated minimal cytotoxic effects on the cells, suggesting significantly reduced anti-cancer activity in these modified forms. The lack of pronounced cytotoxicity in these loaded nano-systems could be due to factors such as changes in nanoparticle size, the interaction dynamics with DOX, and variations in cellular uptake. Additionally,
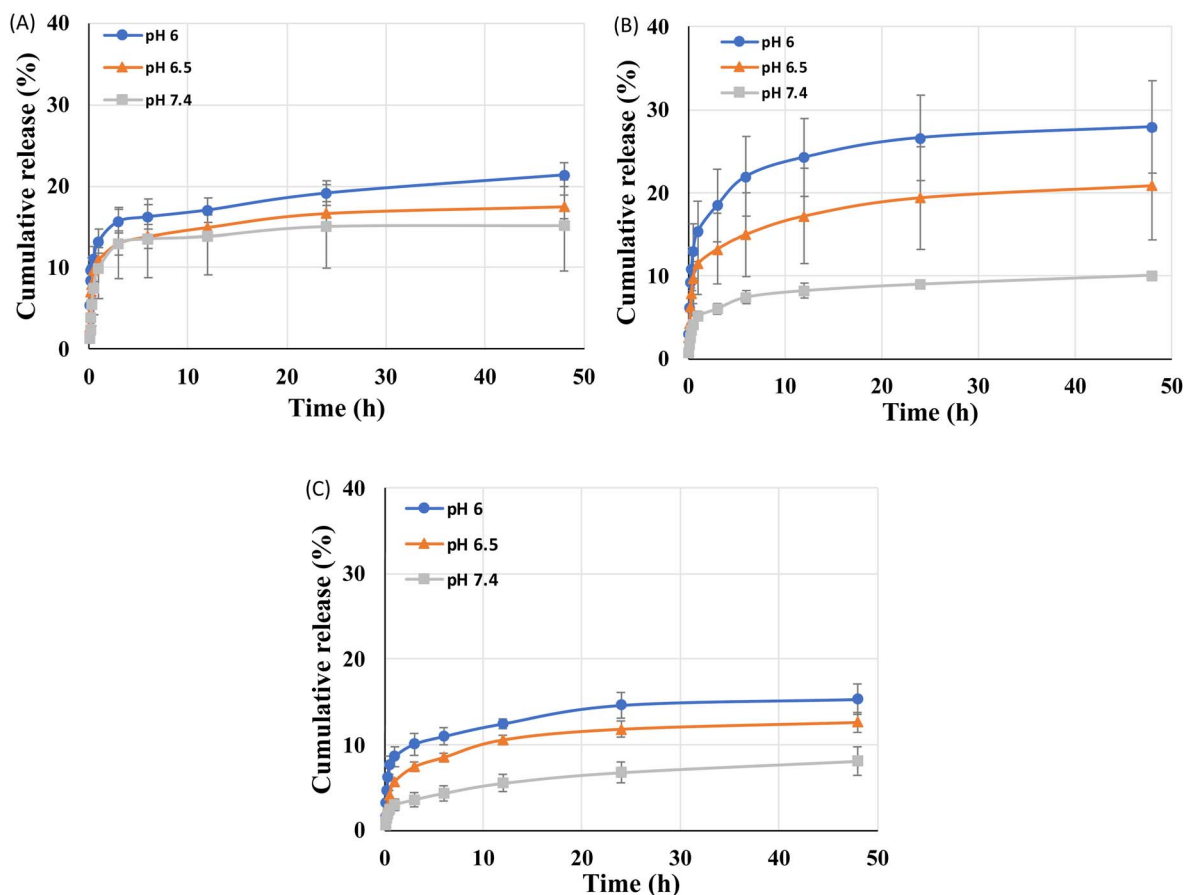

Fig. 5 Cumulative release profile of DOX from: (A) MSNs-PDPA-*co*-PGMA; (B) MSNs-PDPA-*co*-PGMA X-linked with DAE and (C) MSNs-PDPA-*co*-PGMA X-linked with Orn under different conditions.
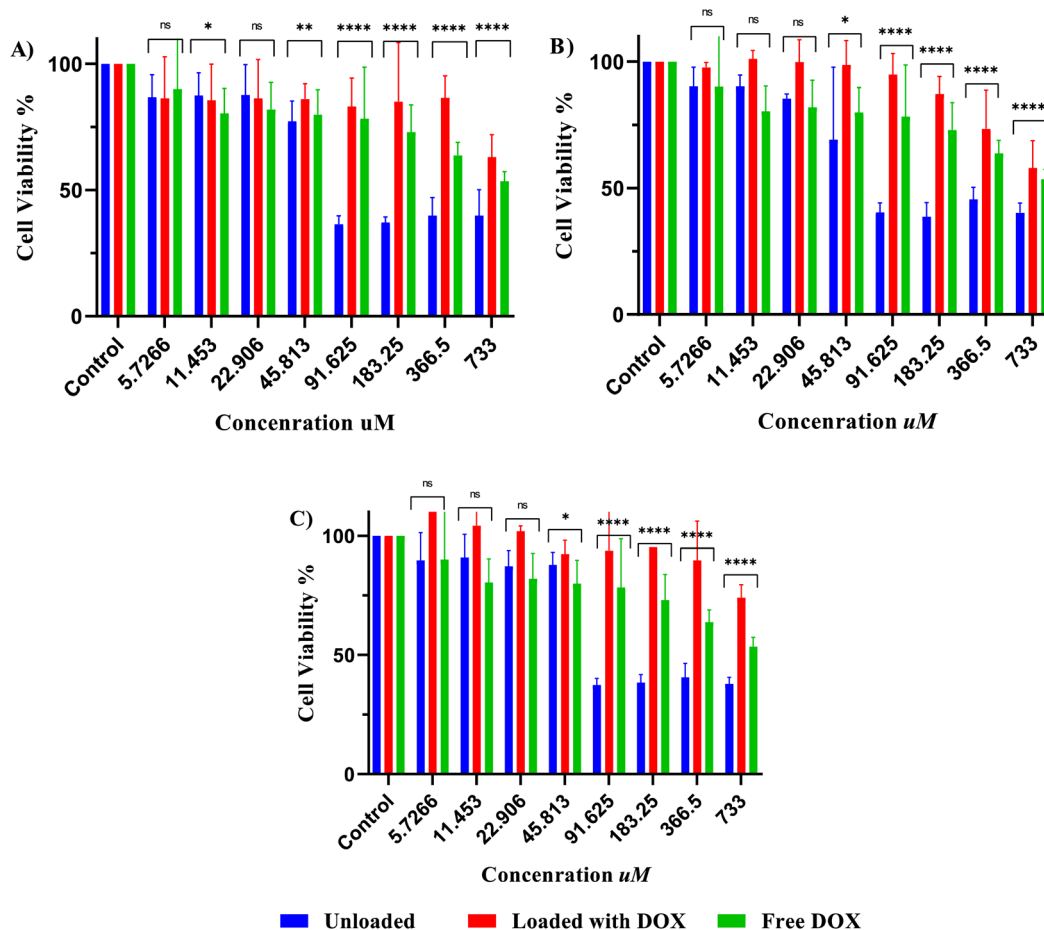
Fig. 6 Cytotoxicity assay by MTT assay Caco2 cell line. Cells were treated with different DOX concentration for 24 h in three different nano systems. (A) MSNs-PDPA-*co*-PGMA. (B) MSNs-PDPA-*co*-PGMA X-linked with DAE. (C) MSNs-PDPA-*co*-PGMA X-linked with Orn. Colors represent unloaded, loaded with DOX and free DOX. Statistical analysis is performed using two-way ANOVA in GraphPad Prism (Version 6.01, Prism.). The treated groups were compared to the control untreated cells group ($p < 0.05$ was considered statistically significant. ns: non-significant).

MSNs-PDPA-*co*-PGMA displayed higher cytotoxicity when loaded with DOX compared to the X-linked variants. This discrepancy underscores the need for further investigation to understand how modifications in the nano-systems influence DOX uptake and release. The cytotoxicity of nanosystems is influenced by their physicochemical properties, including size, hydrophobicity, charge, and interactions.[31] Higher hydrophobicity in nanosystems can result in poor cellular uptake, leading to lower cytotoxic effects.[32] The reduced cytotoxic effects observed in loaded nanosystems could be attributed to the interaction of DOX with the nanoparticles. Additionally, differences in cellular uptake may contribute to the varying cytotoxic effects.[33] The cellular uptake of nanosystems significantly affects their cytotoxic activity, highlighting the need for further investigations to study the uptake of nanosystems containing DOX. In summary, while the unloaded nano-systems showed significant anti-cancer activity, their loaded counterparts, particularly those modified with ornithine and ethylenediamine, did not exhibit comparable anti-cancer effects. This finding points towards the complex interplay between nano-system composition, drug loading, and cytotoxicity, warranting additional studies to elucidate the mechanisms governing these relationships.

4 Conclusion

This study demonstrates the potential of utilizing MSNs-PDPA and MSNs-PDPA-*co*-PGMA nanoparticles, with particle sizes ranging from 63 to 94 nm, as promising drug carriers in cancer treatment. Through surface functionalization and modifications, these nanoparticles acquire pH-responsive properties, enabling controlled release of DOX, a commonly used anticancer drug. The drug release studies revealed an 8 μg mg^{-1} loading capacity, with release rates varying according to pH changes. Intriguingly, cytotoxicity assays demonstrated that unloaded nano-systems induced 60% cell death at concentrations above 45 μM in Caco2 cells, while loaded nano-systems displayed varying cytotoxic effects based on their chemical modifications. This study underscores the importance of nanoparticle design in drug delivery efficacy and anti-cancer activity. Future research should explore the optimization of

nano-systems for enhanced drug delivery and efficacy, aiming to harness the full therapeutic potential of these advanced materials in cancer treatment.

Author contributions

S. Lahmadi, A. Beagan, S Alamery, K. Alotaibi, A. Alswieleh designed and performed the experiments, analyzed the data, wrote the draft paper, and revised the paper.

Conflicts of interest

The authors declare no conflict of interest.

Acknowledgements

References

1 R. Liu, C. Luo, Z. Pang, J. Zhang, S. Ruan, M. Wu, L. Wang, T. Sun, N. Li and L. Han, Advances of nanoparticles as drug delivery systems for disease diagnosis and treatment, *Chin. Chem. Lett.*, 2023, **34**(2), 107518.

2 M. Xu, X. Han, H. Xiong, Y. Gao, B. Xu, G. Zhu and J. Li, Cancer nanomedicine: emerging strategies and therapeutic potentials, *Molecules*, 2023, **28**(13), 5145.

3 Y. Yang and P. Jiao, Nanomaterials and nanotechnology for biomedical soft robots, *Mater. Today Adv.*, 2023, **17**, 100338.

4 P. M. Giri, A. Banerjee and B. Layek, A Recent Review on Cancer Nanomedicine, *Cancers*, 2023, **15**(8), 2256.

5 E. D. Mohamed Isa, H. Ahmad, M. B. Abdul Rahman and M. R. Gill, Progress in mesoporous silica nanoparticles as drug delivery agents for cancer treatment, *Pharmaceutics*, 2021, **13**(2), 152.

6 M. Narvekar, H. Y. Xue, J. Y. Eoh and H. L. Wong, Nanocarrier for poorly water-soluble anticancer drugs—barriers of translation and solutions, *AAPS PharmSciTech*, 2014, **15**(4), 822–833.

7 G. M. Sulaiman, H. M. Waheeb, M. S. Jabir, S. H. Khazaal, Y. H. Dewir and Y. Naidoo, Hesperidin loaded on gold nanoparticles as a drug delivery system for a successful biocompatible, anti-cancer, anti-inflammatory and phagocytosis inducer model, *Sci. Rep.*, 2020, **10**(1), 1–16.

8 S. D. Hettiarachchi, R. M. Graham, K. J. Mintz, Y. Zhou, S. Vanni, Z. Peng and R. M. Leblanc, Triple conjugated carbon dots as a nano-drug delivery model for glioblastoma brain tumors, *Nanoscale*, 2019, **11**(13), 6192–6205.

9 X. Peng, Q. Pan, B. Zhang, S. Wan, S. Li, K. Luo, Y. Pu and B. He, Highly stable, coordinated polymeric nanoparticles loading copper (II) diethyldithiocarbamate for combinational chemo/chemodynamic therapy of cancer, *Biomacromolecules*, 2019, **20**(6), 2372–2383.

10 X. Zhang, L. Meng, Q. Lu, Z. Fei and P. J. Dyson, Targeted delivery and controlled release of doxorubicin to cancer cells using modified single wall carbon nanotubes, *Biomaterials*, 2009, **30**(30), 6041–6047.

11 A. Wani, G. H. L. Savithra, A. Abyad, S. Kanvinde, J. Li, S. Brock and D. Oupický, Surface PEGylation of Mesoporous Silica Nanorods (MSNR): Effect on loading, release, and delivery of mitoxantrone in hypoxic cancer cells, *Sci. Rep.*, 2017, **7**(1), 1–11.

12 P. Dogra, N. L. Adolphi, Z. Wang, Y.-S. Lin, K. S. Butler, P. N. Durfee, J. G. Croissant, A. Noureddine, E. N. Coker and E. L. Bearer, Establishing the effects of mesoporous silica nanoparticle properties on in vivo disposition using imaging-based pharmacokinetics, *Nat. Commun.*, 2018, **9**(1), 1–14.

13 Y. Liu, B. Huang, J. Zhu, K. Feng, Y. Yuan and C. Liu, Dual-generation dendritic mesoporous silica nanoparticles for co-delivery and kinetically sequential drug release, *RSC Adv.*, 2018, **8**(71), 40598–40610.

14 B. Yameen and A. Farrukh, Polymer brushes: Promises and challenges, *Chem. - Asian J.*, 2013, **8**(8), 1736–1753.

15 T. Chen, R. Ferris, J. Zhang, R. Ducker and S. Zauscher, Stimulus-responsive polymer brushes on surfaces: Transduction mechanisms and applications, *Prog. Polym. Sci.*, 2010, **35**(1–2), 94–112.

16 Y. Zhou, C. Chang, Z. Liu, Q. Zhao, Q. Xu, C. Li, Y. Chen, Y. Zhang and B. Lu, Hyaluronic acid-functionalized hollow mesoporous silica nanoparticles as pH-sensitive nanocarriers for cancer chemo-photodynamic therapy, *Langmuir*, 2021, **37**(8), 2619–2628.

17 Y. Zhang, Y. Xing, M. Xian, S. Shuang and C. Dong, Folate-targeting and bovine serum albumin-gated mesoporous silica nanoparticles as a redox-responsive carrier for epirubicin release, *New J. Chem.*, 2019, **43**(6), 2694–2701.

18 M. Dubner, V. J. Cadarso, T. N. Gevrek, A. Sanyal, N. D. Spencer and C. Padeste, Reversible light-switching of enzymatic activity on orthogonally functionalized polymer brushes, *ACS Appl. Mater. Interfaces*, 2017, **9**(11), 9245–9249.

19 M. Du, Y. Chen, J. Tu, C. Liufu, J. Yu, Z. Yuan, X. Gong and Z. Chen, Ultrasound responsive magnetic mesoporous silica nanoparticle-loaded microbubbles for efficient gene delivery, *ACS Biomater. Sci. Eng.*, 2020, **6**(5), 2904–2912.

20 J. Singh and P. Nayak, pH-responsive polymers for drug delivery: Trends and opportunities, *J. Polym. Sci.*, 2023, **61**, 2828–2850.

21 L. H. K. Alfhaid, Recent advance in functionalized mesoporous silica nanoparticles with stimuli-responsive polymer brush for controlled drug delivery, *Soft Mater.*, 2022, **20**(3), 364–378.

22 A. López Ruiz, A. Ramirez and K. McEnnis, Single and Multiple Stimuli-Responsive Polymer Particles for Controlled Drug Delivery, *Pharmaceutics*, 2022, **14**(2), 421.

23 F. Ofridam, N. Lebaz, É. Gagnière, D. Mangin and A. Elaïssari, Polymethylmethacrylate derivatives Eudragit

E100 and L100: Interactions and complexation with surfactants, *Polym. Adv. Technol.*, 2021, **32**(1), 379–390.

24 A. M. Beagan, A. A. Alghamdi, S. S. Lahmadi, M. A. Halwani, M. S. Almeataq, A. N. Alhazaa, K. M. Alotaibi and A. M. Alswieleh, Folic acid-terminated poly (2-diethyl amino ethyl methacrylate) brush-gated magnetic mesoporous nanoparticles as a smart drug delivery system, *Polymers*, 2020, **13**(1), 59.

25 A. Beagan, S. Lahmadi, A. Alghamdi, M. Halwani, M. Almeataq, A. Alhazaa, K. Alotaibi and A. Alswieleh, Glucosamine Modified the Surface of pH-Responsive Poly (2-(diethylamino) ethyl Methacrylate) Brushes Grafted on Hollow Mesoporous Silica Nanoparticles as Smart Nanocarrier, *Polymers*, 2020, **12**(11), 2749.

26 B.-b. Zhang, X.-j. Chen, X.-d. Fan, J.-j. Zhu, Y.-h. Wei, H.-s. Zheng, H.-y. Zheng, B.-h. Wang, J.-g. Piao and F.-z. Li, Lipid/PAA-coated mesoporous silica nanoparticles for dual-pH-responsive codelivery of arsenic trioxide/paclitaxel against breast cancer cells, *Acta Pharmacol. Sin.*, 2021, **42**(5), 832–842.

27 J. Parnian, L. Ma'mani, M. R. Bakhtiari and M. Safavi, Overcoming the non-kinetic activity of EGFR1 using multi-functionalized mesoporous silica nanocarrier for in vitro delivery of siRNA, *Sci. Rep.*, 2022, **12**(1), 17208.

28 G. Thakur, F. C. Rodrigues and K. Singh, Crosslinking biopolymers for advanced drug delivery and tissue engineering applications, *Cutting-Edge Enabling Technologies for Regenerative Medicine*, 2018, pp. 213–231.

29 X. M. Sim, C.-G. Wang, X. Liu and A. Goto, Multistimuli Responsive Reversible Cross-Linking–Decross-Linking of Concentrated Polymer Brushes, *ACS Appl. Mater. Interfaces*, 2020, **12**(25), 28711–28719.

30 Y. Ren, W. Wu and X. Zhang, The feasibility of oral targeted drug delivery: Gut immune to particulates?, *Acta Pharm. Sin. B*, 2023, **13**(6), 2544–2558.

31 S. Lv, M. Li, Z. Tang, W. Song, H. Sun, H. Liu and X. Chen, Doxorubicin-loaded amphiphilic polypeptide-based nanoparticles as an efficient drug delivery system for cancer therapy, *Acta Biomater.*, 2013, **9**(12), 9330–9342.

32 A. Y. Dzhuzha, I. I. Tarasenko, L. I. Atanase, A. Lavrentieva and E. G. Korzhikova-Vlakh, Amphiphilic Polypeptides Obtained by the Post-Polymerization Modification of Poly (Glutamic Acid) and Their Evaluation as Delivery Systems for Hydrophobic Drugs, *Int. J. Mol. Sci.*, 2023, **24**(2), 1049.

33 M. Brzeziński, W. Gonciarz, B. Kost and M. Chmiela, Can histamine cause an enhancement of the cellular uptake and cytotoxicity of doxorubicin-loaded polylactide nanoparticles?, *Eur. J. Pharm. Sci.*, 2023, **185**, 106438.